

Application of a customizable sensor platform to detection of atmospheric gases by UAS

Andrew D. Falabella, *IEEE Member*, David O. Wallin, John A. Lund, *IEEE Member*

Abstract—The dramatic reduction in the cost of consumer unmanned aerial systems (UAS) presents an opportunity for widespread adoption of UAS across several established areas of study. We present the development of a sensor prototyping platform designed to be accessible to a wide variety of industrial, academic, and hobbyist users. We also present a low-cost gas sensor array designed and fabricated using this development platform. Use of common low-cost ceramic metal-oxide gas sensors on a UAS required the inclusion of several supplemental compensation sensors, as well as the development of hardware to mitigate non-ideal impacts of UAS motion on the sensors. The system was tested at a private wetland in Western Whatcom County, WA during autumn 2017 in an effort to detect and geographically map potential methane hotspots, as well as test the development platform. While unable to detect hotspots within a 10-meter radius, flights conducted at 1 m/s provided more consistent detection than those flown at 3 m/s. Further work is required to mitigate non-ideal effects and improve the utility of a low-cost system for data collection by UAS. The sensor development platform, however, successfully supported this test and is suitable for further prototyping.

I. INTRODUCTION

Declines in the cost of UAS as well as improvements in ease of use of these systems have increased the attractiveness of unmanned aircraft to many academic disciplines. Widespread implementation of this technology, however, necessitates the development of new toolkits that lower the barrier of entry to UAS platform development to facilitate broad UAS adoption beyond existing off-the-shelf imaging applications. We report on three related research tasks involving the incorporation of UAS into environmental research. The preliminary effort is the construction of a sensor development and deployment platform tailored for small unmanned aerial system (sUAS) applications. The second is the use of this platform for the development of a methane gas detection system incorporating low-cost ceramic metal-oxide gas sensors as well as a collection of supplemental sensors intended to record correlated environmental data used to correct sensor error. Finally, we report on experimentation with this sensor system to detect low concentrations of methane over wetlands and modifications made both to sUAS flight planning as well as the sensor hardware to mitigate non-ideal effects observed during experimentation.

A. D. Falabella is a student in the Department of Environmental Sciences and the Honors program at Western Washington University, Bellingham, WA 98225 USA (e-mail: drew.falabella@gmail.com).

D. O. Wallin is with the Department of Environmental Sciences, Western Washington University, Bellingham, WA 98225 USA (e-mail: david.wallin@wwu.edu).

J. A. Lund is with the Engineering and Design Department, Western Washington University, Bellingham, WA 98225 USA (e-mail: john.lund@wwu.edu).

A. Unmanned Aerial Systems for Research

UAS, while widely used for image collection, have also been applied to low-altitude atmospheric research such as aerosol measurement [1]. Trace atmospheric gases have only recently begun to receive the same attention [2]. There are multiple advantages to using sUAS rather than ground surveys, including faster sampling times, precise georeferencing, and greater statistical confidence resulting from large sample sizes obtained. Advancements in sUAS applications have great potential to improve research efficiency for environmental sciences as well as expedite infrastructure maintenance. However, obtaining high-quality data during a limited flight time remains a substantial obstacle to effective UAS research, especially in cases where funding is limited. Reduction in the weight of UAS payloads remains a fundamental key to this goal, and is considered in our system design.

B. Comparison to Existing Technology

A variety of existing options are available for prototyping sensor deployments on sUAS. The most common option is development with companion computers intended to communicate with the flight controller to extract telemetry data [3]–[6]. Standard communications protocols (such as MAVLink) minimize the effort required to achieve communication with the host controller. However, the task of sensor deployment with these systems ultimately matches the complexity of development on the companion computer platform, often requiring mastery of C/C++, Java, or Python even to implement the simplest of sensing tasks. Where sUAS systems have been developed with the explicit purpose of enabling academic research projects [7], basic implementations still require the development of source programming using general-purpose programming languages which are not tailored to UAS applications. Often, implementation requires development of software using multiple distinct programming or scripting languages for data acquisition and transmittal as well as API specification. The high burden of foundational programming knowledge makes sensor prototyping inaccessible to many researchers who wish to use UAS-based sensing as a tool for rapid experimentation in fields far detached from engineering and computer science.

Many existing companion computers use off-the-shelf prototyping system such as the Raspberry Pi or Intel Edison, which not only deploy superfluous hardware, but also require separate prototyping hardware and power regulation. The system described herein can be viewed as a lean implementation of an onboard computer where both the hardware and software systems have been stripped down to their basic elements and tailored to sUAS applications. The

result is a low-mass (48g total including regulation and prototyping board) onboard computer with a UAS-specific scripting language that lowers the learning curve for sensor implementation. Users with only minimal knowledge of hardware and software systems can implement autonomous sensing with highly customizable logging with verbose telemetry data, in a matter of minutes.

Looking beyond the sensing platform to the sensors themselves, a variety of sensors currently exist which can be incorporated into UAS. The Figaro TGS 2600 gas sensor, a ceramic metal-oxide sensor (CMOS) [8], has been used in outdoor, stationary applications over a time period of weeks to months [9]. The open-path laser spectroscopy method employed by Cossel et al. [2] eliminates the need for the sUAS to carry a heavy sensing payload, and can detect a wide range of gases in one survey. Another notable implementation employs a laser spectrometer which parlays instrumentation developed for space exploration, minimizing payload weight [10]. This sUAS methane sensor achieved sub-ppm methane detection with only a 400g sensor payload. While this sensor and payload deployment technique are suitable for methane detection, the cost and payload mass still limit sUAS deployment to mainly standalone applications.

II. SENSOR DEVELOPMENT BOARD

We developed a rapid-prototyping platform for deployment of sensor systems on a sUAS which does not require users to implement any low-level programming or embedded systems design. The platform allows users to prototype analog and digital sensor systems in a similar manner to a typical prototyping board and relies on a simple scripting language geared toward sUAS applications to perform periodic sampling of sensor outputs.

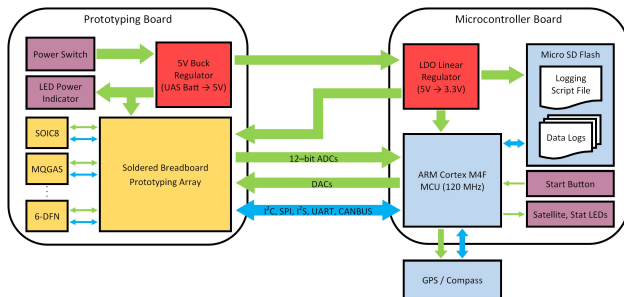


Fig. 1. Customizable sensor development platform architecture with a low-cost replaceable prototyping board (left) and a reusable microcontroller (right) programmed with a UAS-based script interpreter for rapid deployment of sensing and data acquisition.

The architecture of the prototyping platform is shown in Fig. 1. The system consists of a low-cost breakout board with standard 0.1" solder hole spacing as well as footprints for common gas, light, temperature, and other environmental sensors. The board includes holes for vibration isolating elastomer balls commonly used for mechanical decoupling of payloads from the sUAS body. The main breakout board (Fig. 2) also includes a buck regulator capable of switching regulation of a UAS battery voltage down to a 5 V signal with a maximum output current of 3 A. The addition of a separate regulator allows the development platform to not only minimize impact and noise on power sources regulated

by the sUAS, but also limit current draw. In the example presented herein, the supply regulator of the development board is capable of providing 3 A of current regulated to 5 V without exceeding the 1.1 A current limit of the 3DR's accessory connector port connection to the 17 V battery. For the user, this minimizes requirements to modify commercial sUAS and in the case of common commercial sUAS such as the 3DR Solo, no modification is required.

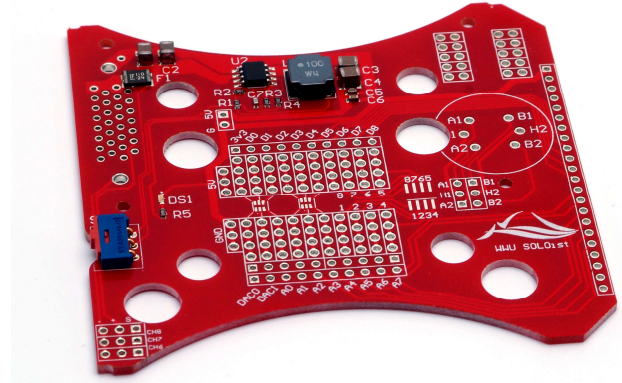


Fig. 2. Sensor development breadboard.

The prototyping board includes connections to a removable ARM Cortex M4 microcontroller. The microcontroller is programmed with a script interpreter that reads a user-defined script from a microSD card and executes commands to acquire GPS data as well as analog and digital data from the prototype board. The script can perform rudimentary data processing and record data to a log file on the SD card. The script command sequence is executable based on a time delay, or on a distance delay which relies on GPS position to trigger sampling. This UAS-focused script approach is designed to mimic behavior familiar to those who use UAS for autonomous flight planning and image acquisition. In addition to logging data based on time or GPS distance, the scripting language includes many UAS-based features such as native single-instruction manipulation of all NMEA GGA and GSA data. Scripts can easily include conditional formatting based upon these data as well, such as pausing data acquisition due to a poor satellite fix or decreasing the sample-by-distance acquisition rate as ground speed increases. User-defined script commands also allow users who wish to incorporate very advance functionality to add initialization and function programming to a collection of pre-named commands that can then be called within the script.

An example of the functionality of this sUAS development platform is shown in Fig. 3. A simple sensor circuit is constructed with a heated metal-oxide gas sensor (MOS), a barometric altimeter, and a temperature sensor. These sensors are powered by the onboard regulated power supply. The inclusion of simple circuit components produces analog sensor signals which are connected to analog inputs of the attached microcontroller board. The script defines the sampling rate (1 sample every 10 meters in the example of Fig. 3) and samples the appropriate analog inputs, then outputs the data to a log file on the SD card with appropriate tab-separated formatting.

Although this simple example illustrates the basic system functionality, the platform is capable of far more powerful sensor incorporation and manipulation. The gas sensor selected for this research required the use of analog sampling, as well as digital control and data collection using multiple I²C-based sensors.

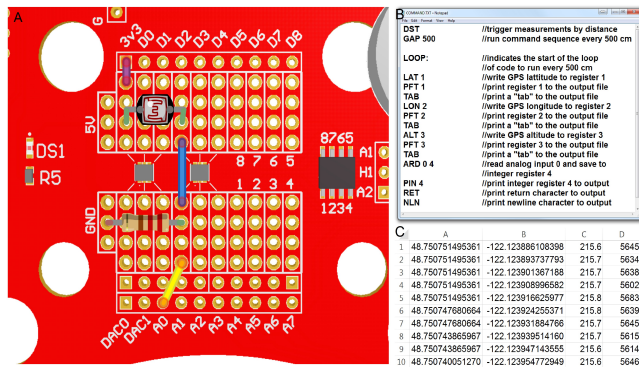


Fig. 3. Example of a simple sensor deployment. Traditional breadboard design for a simple light sensor (A), example script command file to collect analog sensor data and log it along with GPS position data (B), and resulting data log (C).

III. APPLICATION TO GAS DETECTION

Climate scientists gain added value from just-in-time environmental data and would benefit from faster emissions estimates (which proper UAS configuration may provide) to target detailed surveys of potential carbon sources in a natural context. The applications and experimentation descriptions that follow were conducted with these considerations in mind at a wetland in an effort to detect natural concentrations of methane gas (CH₄). However, applications to natural gas infrastructure maintenance or industrial leak detection are also possible. As such, some of the previous work described herein focuses on these applications.

A. Sensing Approach

The Figaro TGS 2600 gas sensor, a ceramic metal-oxide sensor (CMOS), was selected for this work due to its low cost, light weight, and short response time. The 2600 has also been used for methane detection in two prior studies, albeit with different parameters than our own [9][11].

The development of even lighter and lower-cost methane detection techniques for sUAS and UAS applications would not only improve the accessibility of methane sensing, but also allow methane detection down to atmospheric levels as part of a broader plurality of sensors on general purpose gas and environmental detection systems.

Although inexpensive and widely available, the use of MOS redox gas sensors for detection of methane is generally limited due to catalyst transients, non-specific sensitivity (particularly to water and hydrogen), and barometric pressure non-linearity. The TGS 2600 detects gases by monitoring a reduction-oxidation reaction between the gas and surrounding oxygen. This changes the resistance of the SnO₂ element in contact with the gas, which is translated into an analog signal and output to our sensor development board. However, gas selectivity depends on temperature. If the element temperature deviates too much from the 400° C optimum, selectivity for CH₄ may be impacted [12]. As a result, proper

temperature regulation must be used to prevent undesired cooling of the element. Our research effort aims not only to deploy a collection of similarly low-cost and lightweight sensors to identify critical covariant components to MOS redox gas sensors but also to determine whether our sensor development board as detailed above is capable of supporting such an enterprise.

B. Sensor Bundle

Noting the limitation of the TGS 2600 sensor and its sensitivity to temperature, humidity, and barometric pressure, we developed a custom sensor printed circuit board (PCB) which incorporates a collection of analog and digital sensors necessary for methane sensor reading compensation. The sensor board is shown in Fig. 4. The PCB consists of a 0.8 mm thick fiberglass substrate to minimize mass. Necked-down regions of the PCB are to provide thermal isolation between the barometric altimeter (NPX MPL3115), the humidity sensor (Sensirion SHT35), and the methane sensor (Figaro TGS 2600). Both the barometric altimeter and humidity sensor include their own independent temperature sensors; however, the aim of these sensors is to measure air temperature, not PCB temperature which can rise due to thermal conduction from the heated TGS 2600 element.



Fig. 4. Peripheral sensor bundle with gas, relative humidity, and barometric altitude sensors mounted.

C. Regulatory Considerations

Choice of sample site was dictated largely by regulations on UAS imposed by the FAA and Washington State Department of Fish and Wildlife. Easily accessible wetlands that met the biological and chemical criteria for CH₄ emissions were managed by the WDFW, which enforced a strict no-drone policy at the time research was conducted. FAA regulations also prohibited flying at sites within 5 miles of Bellingham International Airport without a waiver, and timing during the undergraduate school year did not allow for a 90-day delay. Two of the authors carried FAA UAS pilot certifications, ensuring compliance with 14 CFR Part 107 during operations at the final site.

D. Wetland Sample Site

Sampling occurred at a private fen in Western Whatcom County WA, south of Deming. The fen is classified as a palustrine scrub-shrub wetland that is seasonally flooded and partially ditched or drained [13]. This would indicate that

hydrologic alteration has occurred on site, but there is sufficient moisture to support hydrophytes. Our initial survey on foot revealed that over 0.5 m of standing water existed over a substantial part of the wetland even in July, near the height of the Pacific Northwest drought season, and may satisfy the appropriate biogeochemical requirements for methane generation in the sediments. Notable hydrophytic vegetation included Reed Canary grass (*Phalaris arundinacea*) which contains aerenchyma tissue used to vent harmful gases and allow aeration of submerged root tissues [14]. A small water inlet provided nutrient transport from the northwest, but little-to-no outlet flow was observed.

E. Biochemical Indication and Detection of Emissions

Methane is often generated in the anoxic conditions of submerged sediments, but only when reduction chemistry is capable of reducing carbon rather than more preferable electron receptors such as nitrogen, iron, or sulfur [15]. Thus, methanogenesis requires the absence or inaccessibility of those receptors. Based on its hydrology, vegetation, and available detritus for carbon input to the soil column, the sample site meets a number of important criteria for methanogenesis.

The TGS 2600 detects gases by monitoring a reduction-oxidation reaction between the gas and surrounding oxygen. This changes the resistance of the SnO₂ element in contact with the gas, which is translated into an analog signal and output to our sensor development board. However, gas selectivity depends on temperature. If the element temperature deviates too much from the 400° C optimum, selectivity for CH₄ may be impacted [12]. As a result, proper temperature regulation must be used to prevent undesired cooling of the element.

F. Quadcopter and hardware configuration

A 3DRobotics Solo quadcopter was chosen as a base for the methane sensor sUAS. An accessory port on the ventral side allows our sensor array to draw power directly from the Solo, and its removable batteries are swappable in minutes in the field. It is also compatible with autonomous flight planning, which was carried out through the open-source Mission Planner software [16].

The sensor board and microprocessor were mounted to the ventral side of the Solo (Fig. 5), while the sensor packages were enclosed in two perforated, 3D-printed plastic shells (Fig. 6), each on the tip of its own 0.6 m fiberglass boom extending to the front or rear of the quadcopter. This consideration was intended to shield the gas sensor elements from cooling by the wind and clear them from the influence of the downward prop wash near the fuselage of the sUAS. The need to isolate the sensors from air perturbations to minimize convection cooling while also ensuring sufficient gas circulation to reduce detection transients; this is later addressed through the reduction of transversal velocity during flight. Connections from the development board to the sensor booms were accomplished with ribbon cable, reducing the potential for snags while allowing branching of individual wires at the board. Plastic connectors (2 mm Sherlock, Molex) were used to allow easy component replacement in case of damage.



Fig. 5. Top: sensor development board connected to the ventral side of the UAS, alongside the fiberglass booms and ribbon cable. Bottom: Fully-equipped UAS displayed before conducting a sample flight

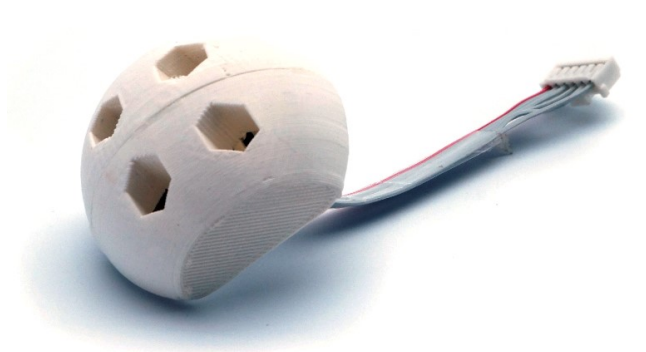


Fig. 6. Peripheral sensor bundle (Fig. 4) enclosed in a 3D-printed, protective shell. This consideration is intended to prevent excess cooling of the sensor and resulting reduction in sensitivity to CH₄.

G. Flight Methods

Sampling was conducted at the private wetland site between September and November, 2017. Two autonomous flight plans were tested, differing by coverage and flight speed. The sUAS was allowed to sample from ground level for 1 – 5 minutes before and after each flight. After its preliminary sampling period, the sUAS was manually piloted to its starting point near the center of the wetland, where autonomous mode was engaged and a cross-grid pattern flown. Autonomous flight was terminated upon experiencing a low battery condition or when the flight plan was completed, whichever came first, at which point the pilot would take action. The sUAS was landed manually and allowed to complete its end-of-flight sampling as well. Data

was reviewed on the laptop base station between flights. Finally, the microSD card was returned to the sUAS and its battery replaced to repeat the process for the next flight. The prototyping board remained powered through a USB connection to keep the gas sensors warm and avoid thermal transients for the subsequent flight.

September flights covered a 13,800 m² area above the fen at a 3 m/s ground speed (Fig. 7), but October flights used the second flight plan (Fig. 8), covering a smaller area of 3,100 m² at 1 m/s in an attempt to determine whether substantial sensor latency existed that might act as a confounding factor. Another advantage of reduced ground speed is a reduction in gas convection within the baffled sensor enclosure shells, minimizing convection cooling. The latter tests also oriented the sUAS in a single direction during flight to prevent sudden turning (and therefore wind cooling) of the sensor shells. Both plans followed cross-grid patterns with ~10-meter spacing between paths, and were flown at 10 meters above ground level. These methods will be compared to assess relative efficacy.

H. Flight Methods

Sampling was conducted at our private wetland site between September and November, 2017. Two autonomous flight plans were tested, differing by coverage and flight speed. The sUAS was allowed to sample from ground level for 1 – 5 minutes before and after each flight. After its preliminary sampling period, the sUAS was manually piloted to its starting point near the center of the wetland, where autonomous mode was engaged and a cross-grid pattern flown. Autonomous flight was terminated upon experiencing a low battery condition or when the flight plan was completed, whichever came first, at which point the pilot would take action. The sUAS was landed manually and allowed to complete its end-of-flight sampling as well. Data was reviewed on the laptop base station between flights. Finally, the microSD card was returned to the sUAS and its battery replaced to repeat the process for the next flight. The prototyping board remained powered through a USB connection to keep the gas sensors warm and avoid thermal transients for the subsequent flight.

September flights covered a 13,800 m² area above the fen at a 3 m/s ground speed (Fig. 7), but October flights used the second flight plan (Fig. 8), covering a smaller area of 3,100 m² at 1 m/s in an attempt to determine whether substantial sensor latency existed that might act as a confounding factor. Another advantage of reduced ground speed is a reduction in gas convection within the baffled sensor enclosure shells, minimizing convection cooling. The latter tests also oriented the sUAS in a single direction during flight to prevent sudden turning (and therefore wind cooling) of the sensor shells. Both plans followed cross-grid patterns with ~10-meter spacing between paths, and were flown at 10 meters above ground level. These methods will be compared to assess relative efficacy.

I. Flight Data Analysis

Analog output from the TGS 2600 sensors was converted in a multi-step process using the equations from Eugster and Kling [9] to provide an estimate of actual CH₄ concentration,

starting with sensor voltage (V) out from the analog output and 3.3 volts in:

$$V_{out} = \frac{\text{Analog output} * V_{in}}{32,768 \text{ bytes}} \quad (1)$$

Sensor resistance R_s was then obtained from sensor voltages and load resistor value R_l [8]:

$$R_s = \frac{R_l * V_{in}}{V_{out}} - R_l \quad (2)$$

Where V_{in} remains at 3.3 V, R_l is our load resistor of 10 k Ω , and V_{out} is the TGS 2600 output voltage calculated previously. This gives rise to the following, which was used in practice for our system.

$$R_s = \frac{10k\Omega * 3.3 V_{in}}{V_{out}} - 10k\Omega \quad (3)$$

Equation (3) was used to calculate R_s at every point collected from the sample flight as well as clean-air reference R_0 , which was calculated as the mean of R_s values observed during the baseline rest period of one or more minutes before launch for each flight. The ratio R_s/R_0 does not account for relative humidity (RH) or temperature influence, however. We rely on the following two equations from Eugster and Kling to estimate CH₄ concentration in situ:

$$\frac{R_s}{R_{0_{corr}}} = \frac{R_s}{R_0} * [0.024 + (0.0072 * RH) + (0.00246 * C^\circ)] \quad (4)$$

This corrected ratio was then translated into an estimated CH₄ concentration.

$$[CH_4] = (1.82 \pm 0.0005) + (0.0288 \pm 0.0002) * \frac{R_s}{R_{0_{corr}}} \quad (5)$$

In an attempt to consistently monitor hotspots, time series data for estimated methane concentration were plotted in Microsoft Excel, where a tailored linear baseline correction was applied to eliminate time-dependent sensor drift for each flight. The resulting “residuals plot” of each flight was then analyzed by quality control chart: the baseline value was the average methane concentration measured while the sUAS was in autonomous mode over the wetland, and points more than one standard deviation (for that same autonomous flight period) above the baseline value were considered potential hotspots.

Data were imported into ESRI ArcMap 10.5.1 as point feature classes along with satellite imagery of the area from USGS Earth Explorer [17]. GNSS coordinates in the WGS 1984 (G1170) system were projected into the NAD 1983 coordinate Data points where the baseline-corrected methane estimate exceeded the upper bound on the quality control chart (Fig. 10) were selected for the map. These highlighted points were then inspected for patterns.

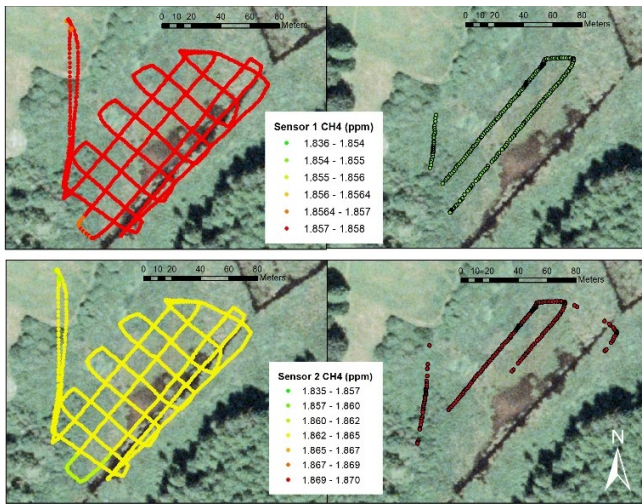


Fig. 7. Sample data from one flight on 12 September. CH₄ concentration is estimated and color-coded on the left as per equations by Eugster and Kling. Right-hand panels show points that meet our definition of a potential hotspot. Colored points in those panels indicate front versus rear sensors only.

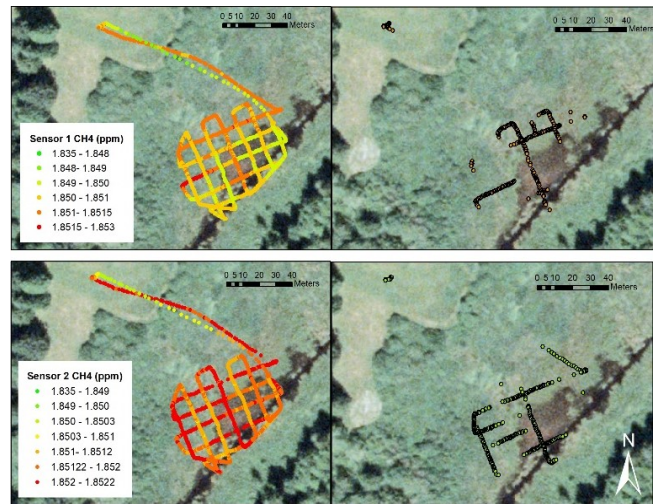


Fig. 8. Sample data from one flight on 31 October. CH₄ concentration is estimated and color-coded on the left as per equations by Eugster and Kling. Right-hand panels show points that meet our definition of a potential hotspot. Colored points in those panels indicate front versus rear sensors only.

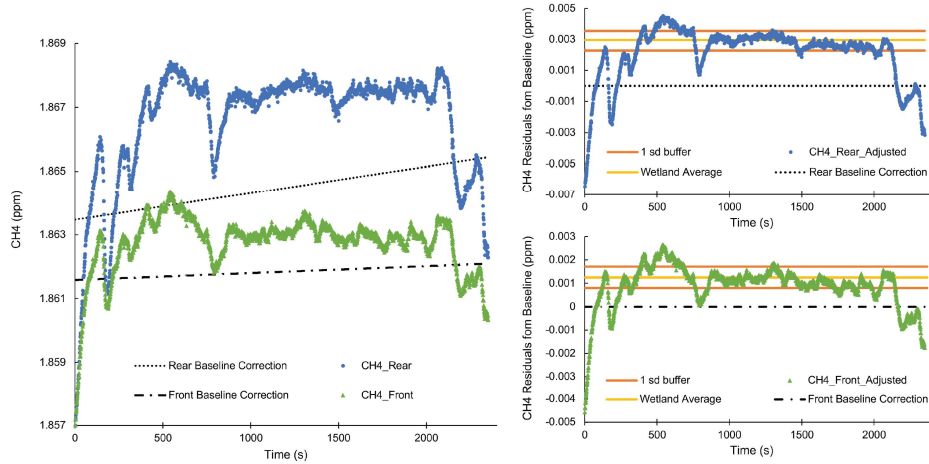


Fig. 9. Estimated ppm CH₄ from the above September flight as a time series. Top row: uncorrected sensor estimates. Bottom row: linear baseline-corrected data with 1-standard deviation buffer lines in orange.

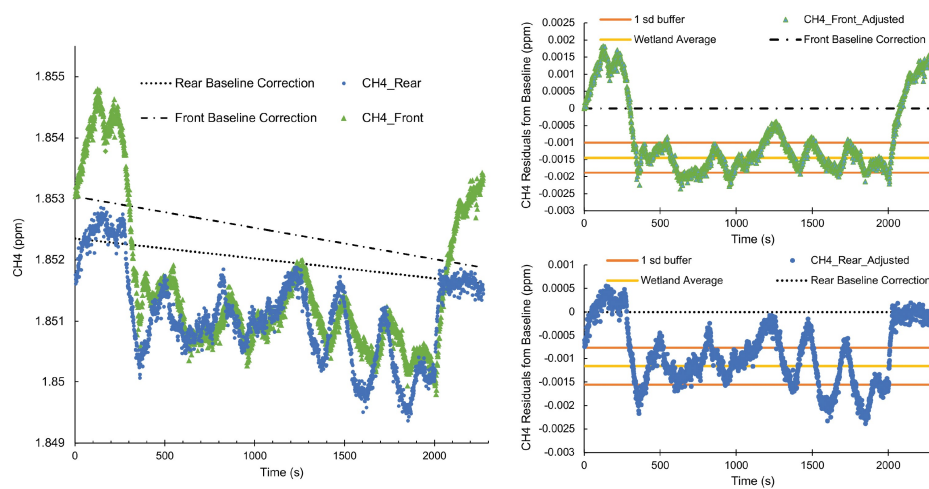


Fig. 10. Estimated ppm CH₄ from the above October flight as a time series. Top row: uncorrected sensor estimates. Bottom row: linear baseline-corrected data with 1-standard deviation buffer lines in orange.

IV. RESULTS

A. Flight Data

Three September test flights at our sample site indicated 1-2 continuous “hotspots,” per our definition, that ran the length of the sampling area rather than staying clustered in smaller areas (Fig. 7). CH₄ concentration estimates ranged from 1.835 to 1.870 ppm, all below the global mean as of August 2017 [18]. When plotted as a function of time, concentrations of CH₄ while in autonomous mode exceeded those measured at ground level before and after flights (Fig. 9). Small perturbations existed in all three flights as well, but most did not exceed the 1-standard deviation buffer after baseline correction was applied.

Flights performed in October with the smaller, slower flight plan revealed discrete hotspots across the wetland which were linear in nature but did not consistently span the entire site (Fig. 8). October field CH₄ concentration estimates ranged from 1.835 – 1.852 ppm. Sensors 1 and 2 did not exhibit predictable sensor drift, though baseline corrections were necessary for all October flights (Fig. 10).

B. System Performance

In addition to logged sensor data, logistic and technical information on system performance was obtained. When properly used, the development board and connected sensors consistently log data as described as long as the UAS continues to deliver power. When some of the wiring to one sensor boom was disconnected in a rough landing, the GNSS and remaining wired sensors continued to collect data. The development board and sensors also weathered moderate wind and drizzle conditions without system failure.

Front and rear sensors appeared to exhibit divergent behavior during September flights. While not visible in Fig. 9, other datasets from September indicate that the front sensor would typically form a downward trend in ppm CH₄ while the rear would start at its lowest point and then enter a “plateau” with a small, positive slope. October flights (example Fig. 10) showed no such divergence between front and rear gas sensors.

V. DISCUSSION

The goal of this research effort was two-fold: the development of a platform for rapid development and deployment of UAS-based sensor systems, and the use of that development platform to apply techniques developed to improve the resolution of low-cost ceramic metal-oxide gas sensors in a laboratory environment to a UAS environment. The first goal was successful – the engineered development platform allows for the rapid deployment of complex collections of analog and digital sensors and circuits with both time and distance triggered sampling using only a simple script. This development platform decouples sensor deployment from the challenges of embedded systems development and lowers the bar to UAS-based sensor deployment. The data collection aspect was also successful. By combining humidity, temperature, and barometric pressure sensors alongside a ceramic metal-oxide gas sensor, and incorporating thermally-insulating but gas permeable enclosure shells, we were able to drive the sensor

measurement range far closer to ambient methane detection while still maintaining a low-cost and lightweight sensor package. This research also led to the development of techniques useful for deployment of this class of sensors on UAS, including the need to maintain external power to the sensor module to minimize thermal transients.

Data collected in September was unhelpful in locating emissions hotspots at the wetland. The points which qualified as potential hotspots under our 1-standard deviation system were strung together for nearly the entire length of the wetland, albeit on only the southeast side. In addition, there was substantial drift in estimated CH₄ such that a single-color symbology system for all three flights proved incapable of illustrating the nuance within each individually when mapped (Fig. 7).

While October flight data contained spikes in CH₄ concentrations that meet our definition for a potential hotspot, these did not appear consistently in a spatial analysis (Fig. 8). While potential hotspots could potentially be centered over the southwest portion of the sampling area, there are still uncertainties associated with these measurements. While flights occurred under near-quiet conditions, 1 m/s might not be slow enough to allow adequate time for the sensor to respond to changes in gas concentration. The reduction in flight speed from September to October may have contributed to the improvements in hotspot clarity and agreement between front and rear sensor readings.

VI. CONCLUSION AND FUTURE WORK

While incapable of highly accurate methane measurement at atmospheric levels, the TGS 2600, when coupled with humidity and temperature sensors to correct for environmental effects, can detect changes in gas concentration at high resolution. Relative changes in emissions seem plausibly within the wetlands emission range observed by Eugster and Kling at Toolik Lake, AK [9]. As such, while the absolute measured concentration may differ flight-to-flight, baseline corrections may be performed to tease out hotspots as compared to the natural, baseline concentration of methane. Downsides of the TGS 2600 are significant, however. The final sensor characteristics are presumably dependent on the effectiveness of the 7-day initial “burn-in” period, as well as the time between power on and the start of experimentation. Sensors underestimated atmospheric concentrations of methane by 0.02 – 0.05 ppm based on the August 2017 average, which indicates inability to detect absolute emissions of 30 ppb on the scale Eugster and Kling suggest.

There are several opportunities to improve performance of this sensor application in the future. A slower flight speed or changes to the sensor shell design might improve ventilation to the sensors and their response time. Unfortunately, each has its cost; reducing flight speed reduces the area a single flight can cover, and shell modifications must be made without exposing the sensor to fast air currents that might cool the heated SnO₂ element. However, upgrades to the sensor package may circumvent some of these problems. The newer Figaro TGS 2611, employed by Van den Bossche et al. in air pollution studies of their own, demonstrated improved filtering hardware over the TGS 2600, resulting in

higher selectivity for methane over other gases [11]. Structural improvements such as strengthening and weatherproofing solder connections would reduce the likelihood of damage in the field. Thorough calibration of sensors in a sterile lab environment may also provide further insight.

Beyond methane gas, however, the performance of relative humidity, temperature, and pressure sensors onboard the existing UAS indicate potential for detection of other environmental hazards. CMOS sensors such as the TGS 2600 are capable of detecting a number of chemically-reducing gases, which may prove useful in detecting hazardous material leaks as well as naturally-occurring compounds. However, the flexibility of the sensor development board allows customization for any number of applications where miniaturized sensors may be used. Further research built on this platform will focus on improving system protection and performance, and expanding the sensor bundle for environmental and infrastructure monitoring purposes.

ACKNOWLEDGMENT

This work was funded by the Office of Research and Sponsored Programs at Western Washington University and by a grant from the Whatcom Community Foundation.

REFERENCES

- [1] J. M. Brady, M. D. Stokes, J. Bonnardel, and T. H. Bertram, "Characterization of a Quadrotor Unmanned Aircraft System for Aerosol-Particle-Concentration Measurements," *Environ. Sci. Technol.*, vol. 50, no. 3, pp. 1376–1383, 2016.
- [2] K. C. Cossel, E. M. Waxman, F. R. Giorgetta, M. Cermak, I. R. Coddington, D. Hesselius, S. Ruben, W. C. Swann, G.-W. Truong, G. B. Rieker, and N. R. Newbury, "Open-path dual-comb spectroscopy to an airborne retroreflector," *Optica*, vol. 4, no. 7, p. 724, 2017.
- [3] W. Zhou, D. Nair, O. Gunawan, T. van Kessel, and H. F. Hamann, "A testing platform for on-drone computation," in *Computer Design (ICCD), 2015 33rd IEEE International Conference on*, 2015, pp. 732–735.
- [4] J. P. Carvalho, M. A. Jucá, A. Menezes, L. R. Olivi, A. L. M. Marcato, and A. B. dos Santos, "Autonomous uav outdoor flight controlled by an embedded system using odroid and ros," in *CONTROL 2016*, Springer, 2017, pp. 423–437.
- [5] P. Burdziakowski, "Low cost hexacopter autonomous platform for testing and developing photogrammetry technologies and intelligent navigation systems," in *Environmental Engineering 10th International Conference., Vilnius*, 2017.
- [6] L. Meier, D. Honegger, and M. Pollefeys, "PX4: A node-based multithreaded open source robotics framework for deeply embedded platforms," in *Robotics and Automation (ICRA), 2015 IEEE International Conference on*, 2015, pp. 6235–6240.
- [7] H. D. Mathias, "An autonomous drone platform for student research projects," *J. Comput. Sci. Coll.*, vol. 31, no. 5, pp. 12–20, 2016.
- [8] Figaro USA, "TGS 2600 - for the detection of Air Contaminants." 2013.
- [9] W. Eugster and G. W. Kling, "Performance of a low-cost methane sensor for ambient concentration measurements in preliminary studies," *Atmos. Meas. Tech.*, vol. 5, no. 8, pp. 1925–1934, 2012.
- [10] B. J. Smith, G. John, L. E. Christensen, and Y. Chen, "Fugitive methane leak detection using sUAS and miniature laser spectrometer payload: System, application and groundtruthing tests," in *Unmanned Aircraft Systems (ICUAS), 2017 International Conference on*, 2017, pp. 369–374.
- [11] M. van den Bossche, N. T. Rose, and S. F. J. De Wekker, "Potential of a low-cost gas sensor for atmospheric methane monitoring," *Sensors Actuators, B Chem.*, vol. 238, pp. 501–509, 2017.
- [12] X. Liu, S. Cheng, H. Liu, S. Hu, D. Zhang, and H. Ning, "A Survey on Gas Sensing Technology," *Sensors*, vol. 12, no. 7, pp. 9635–9665, 2012.
- [13] U.S. Fish and Wildlife Service, "National Wetlands Inventory: Wetlands Data by State," 2017. [Online]. Available: <https://www.fws.gov/wetlands/data/state-downloads.html>. [Accessed: 22-Nov-2017].
- [14] S. Lavergne and J. Molofsky, "Reed canary grass (*Phalaris arundinacea*) as a biological model in the study of plant invasions," *Critical Reviews in Plant Sciences*, vol. 23, no. 5, pp. 415–429, 2004.
- [15] W. J. Mitsch and J. G. Gosselink, *Wetlands*, vol. 5, 2015.
- [16] M. Osborne, "Mission Planner Documentation," 2016. [Online]. Available: <http://ardupilot.org/planner/docs/mission-planner-overview.html>. [Accessed: 11-Jun-2017].
- [17] United States Geological Survey, "USGS EarthExplorer," 2017. [Online]. Available: <https://earthexplorer.usgs.gov/>. [Accessed: 04-Oct-2017].
- [18] E. J. Dlugokencky, "Trends in Atmospheric Methane," *NOAA/ESRL*, 2017. [Online]. Available: https://www.esrl.noaa.gov/gmd/ccgg/trends_ch4/. [Accessed: 22-Nov-2018].